



Cite this: *CrystEngComm*, 2023, 25, 6388

## Advances in protein solubility and thermodynamics: quantification, instrumentation, and perspectives

Joana Ferreira <sup>ab</sup> and Filipa Castro <sup>\*cd</sup>

While protein crystallization has broadly been applied to determine the 3D structure of proteins, it has recently drawn great attention to replace the traditional downstream processing for protein-based biopharmaceuticals due to its advantages in stability, storage, and delivery. However, establishing the crystallization conditions of a protein remains a challenge because of the limited understanding of the underlying phenomena. This highlight provides a critical review of the advanced experimental approaches to measure thermodynamic parameters (e.g. solubility) that can help in establishing the necessary conditions to perform a protein crystallization trial. Firstly, methods and techniques to assess protein crystallizability and solution quality are presented. Next, methodologies to measure the main thermodynamic parameters are revised (with the respective advantages, limitations, and studied proteins). Later, protocols and set-ups (with a focus on microfluidic devices) used to quantify solubility parameters are highlighted (involved apparatus capabilities, solubility screening details, and studied proteins). Lastly, future directions and outlook of this critical review are approached by covering new trends in the research field.

Received 28th July 2023,  
Accepted 10th October 2023

DOI: 10.1039/d3ce00757j

[rsc.li/crystengcomm](http://rsc.li/crystengcomm)

<sup>a</sup> CEFT – Transport Phenomena Research Center, Department of Chemical Engineering, Faculty of Engineering, University of Porto, Rua Dr. Roberto Frias, 4200-465 Porto, Portugal

<sup>b</sup> ALiCE – Associate Laboratory in Chemical Engineering, Faculty of Engineering, University of Porto, Rua Dr. Roberto Frias, 4200-465 Porto, Portugal

<sup>c</sup> CEB – Centre for Biological Engineering, University of Minho, Campus de Gualtar, 4710-057 Braga, Portugal. E-mail: [d6314@ceb.uminho.pt](mailto:d6314@ceb.uminho.pt)

<sup>d</sup> LABBELS – Associate Laboratory in Biotechnology, Bioengineering and Microelectromechanical Systems, University of Minho, Campus de Gualtar, 4710-057 Braga, Portugal



**Joana Ferreira**

Joana Ferreira is a post-doctoral researcher at the Transport Phenomena Research Centre (CEFT) of the Faculty of Engineering of the University of Porto (FEUP). After a master's in chemical engineering at FEUP, she started a joined PhD thesis at KU Leuven and FEUP. Her PhD work was focused on the study of protein crystallization in droplet-based microfluidics. Her research interests in crystal engineering rely on

multidisciplinary perspectives to solve problems through the combination of experimental, numerical, and analytical approaches. Her work was recently highlighted in the virtual issue on Women Researchers at the Forefront of Crystal Engineering of the *Crystal Growth & Design* journal.



**Filipa Castro**

Filipa Castro is an assistant researcher at the Centre of Biological Engineering (CEB) of the University of Minho. She received her PhD thesis from the University of Minho in Bioengineering through the MIT-Portugal programme. The work was done in collaboration with the University of Minho, the Faculty of Engineering of the University of Porto (FEUP) and the Massachusetts Institute of Technology (MIT). After two post-

doctoral fellowships, she joined as a junior researcher the Supramolecular Assemblies group from the Laboratory for Process Engineering, Environment, Biotechnology and Energy (LEPABE) of FEUP, where she deepened her knowledge on crystallization/precipitation science and multiphase flow reactors. She has been studying both fundamentals and applications of crystallization/precipitation science, in particular protein crystallization with applications to both health issues and downstream processing.



# 1. Introduction

Protein crystallization has had an extraordinary impact on the determination of 3D protein structures through X-ray crystallography.<sup>1,2</sup> Over 85% of the protein structures deposited in the Protein Data Bank (PDB) are from crystal-based structural methods.<sup>3</sup> Although other techniques have emerged (*e.g.* Cryo-EM, NMR), X-ray crystallography remains the predominant method to obtain information on protein structures.<sup>4</sup> The information obtained is used for understanding disease mechanisms, identifying drug targets, and optimizing pharmaceutical drug design.<sup>5</sup> Moreover, the pharmaceutical industry has increased efforts for the development of protein crystal-based therapeutics. On the one hand, crystallization can represent a cost-effective alternative to the conventional chromatographic steps in the downstream processing of therapeutic proteins.<sup>6</sup> On the other hand, protein crystals offer advantages in terms of formulation and drug delivery.<sup>7,8</sup> The outstanding impact of protein crystallization over the last decades can be seen from the high number and exponential increase on the number of publications in this research field as shown in Fig. 1.

Regardless of the ultimate purpose, the first step consists in establishing the protein crystallization conditions.<sup>9</sup> This is a challenging task due to the size, complexity and dynamic behaviour of proteins, as well as the intricacy of all the occurring interactions (*i.e.* protein–protein interactions, protein–solvent interactions, *etc.*).<sup>10</sup> Additionally, the unavailability of generalized strategies to crystallize proteins makes the process of identifying crystallization conditions time consuming, fastidious, and costly. Despite the advances of protein screening methods [*i.e.* high-throughput crystallization screening (HTS)], the task of finding crystallization conditions for a specific protein still largely relies on empirical results rather than on theoretical perspectives.<sup>6</sup> A significant number of experiments, where numerous chemical and physical parameters are tested, are mostly conducted. Moreover, it must be done on a recurring basis for each protein under study. According to Newman

*et al.* (2012),<sup>11</sup> only 0.2% of individual crystallization screening conditions performed in HTS laboratory yield a crystal.

Considering the limited understanding of the underlying phenomena, limited guidance is available to systematically identify conditions that may lead to protein crystals. Added to this is the lack of consistency in the reported crystallization conditions, and the limited quantitative experimental data available in the literature. For the crystallization process to take place, the protein must be crystallizable, the quality of the protein solution must be high, and the supersaturation must be achieved.<sup>12</sup> Therefore, the measurement of parameters related to the protein itself (*i.e.* amino acid sequence, folding, *etc.*) and the protein solution (*i.e.* purity, homogeneity, *etc.*), as well as the protein thermodynamics (*i.e.* solubility) system under study is a critical step towards a more rational approach for the establishment of protein crystallization conditions. This rational approach will enable researchers to enhance the crystallization success rate and process controllability, thus drastically reducing screening time and associated costs. In terms of industrial relevance, this will also benefit drug development and crystal-based therapeutics.

Solubility is probably the most important parameter when studying a solid compound since it governs the crystallization process<sup>13</sup> and is a prerequisite to any meaningful crystallization measurement.<sup>14</sup> Saridakis & Chayen (2003)<sup>15</sup> stated that the solubility curve derivation requires at least two conditions (one of which is typically the protein concentration) within a time range around 3–4 weeks. As far as we know, this highlight merges, for the first time, a critical review of the main experimental methodologies and analytical models, as well as applied protocols and instrumentation to determine protein solubility and other thermodynamic parameters that assess protein–protein interactions. This contribution will serve as a guideline for young researchers and academics to identify thermodynamically possible conditions for crystallizing proteins. The covered methods and techniques are focused on soluble proteins.

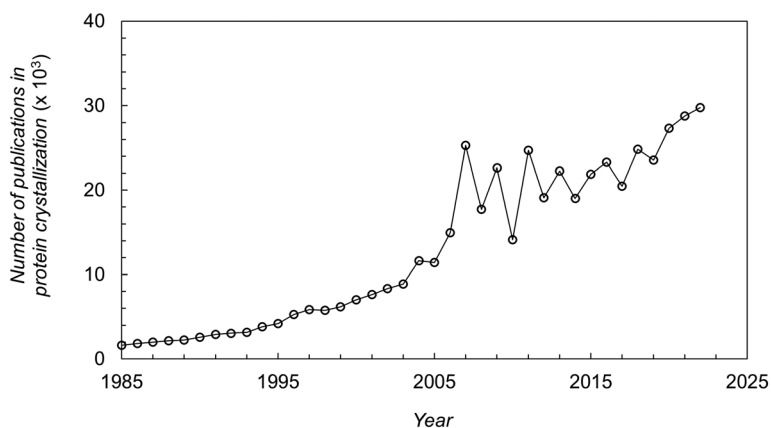


Fig. 1 Number of publications (papers, books, chapters, *etc.*) in protein crystallization reported in the literature over the last decades.<sup>16</sup>



## Highlight

## 2. Protein crystallizability

The protein itself and the protein solution are the most important variables when attempting to perform a crystallization trial.<sup>12,17</sup> Concerning the ability of a protein to bind to partners, the molecular surface structure (e.g. hydrophobicity, charge, amino acid residues) dictates the molecular interactions.<sup>10</sup> According to Derewenda (2010),<sup>18</sup> on the one hand, the surface properties must enable the dissolution of the protein to reach supersaturation, and on the other hand, mediate viable intermolecular contacts. Further, the “quality” of the protein solution is critical to increase the chances of yielding crystals. In general, pure, stable, soluble and monodisperse (*i.e.* uniform population of molecular species) proteins in high concentrations (5–15 mg mL<sup>-1</sup>) are easier to crystallize.<sup>19</sup>

## 2.1. Protein ability to crystallize

The ability of a protein to self-assemble into a crystal is the first requirement for protein crystallization.<sup>12,20</sup> This is specific for each protein under a particular set of conditions and is related to its amino acid sequence and structure. Protein–protein interactions promoting crystal contacts are mainly governed by hydrogen bonds, hydrophobic interactions/van der Waals and electrostatic bonds (Fig. 2). Nevertheless, those interactions are complex, particularly due to protein anisotropy (*i.e.* non-spherical shape, non-uniform charge distribution, rough local topography, and heterogeneous functionality on the protein surface) (Fig. 3), and it is difficult to determine the contribution from each type of interaction.<sup>21,22</sup> One approach to predict the intermolecular interactions of a protein that are likely to be crystal contacts is to use information from protein structure. There are three major techniques to determine the structure of a protein: X-Ray crystallography (XRD), nuclear magnetic resonance (NMR), and electron microscopy (EM). However, knowledge of the crystallization conditions is required.

Derewenda (2010)<sup>18</sup> reported two main criteria that proteins must meet to crystallize: ability to dissolve and ability to enable crystal contacts. The molecular surface of the protein should allow adequate solubility to achieve the requisite supersaturation levels. The residues exposed on the protein surface should promote the compatibility with the environment under study.<sup>25</sup> For instance, polar residues on a protein surface promote the protein's solubility in a polar aqueous solvent. As illustrated in Fig. 3, HEWL has a rather hydrophilic surface which contributes to HEWL's solubility in water. Concerning crystal contacts, studies have related protein surface properties to crystallization propensity.<sup>26–30</sup> Price *et al.* (2010)<sup>30</sup> analyzed the relationship between the frequency of each amino acid, mean hydrophobicity, mean sidechain entropy, total and net electrostatic charge, isoelectric point (pI), the fraction of disordered residues and chain length, and successful protein crystallization (Fig. 4). The results showed that the frequency of certain amino acids

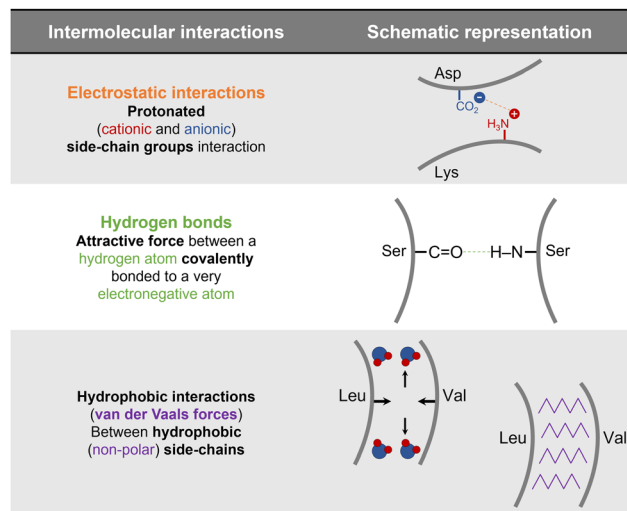


Fig. 2 Schematic representation of the main protein–protein interactions involved in crystal contacts with examples of amino acid residues that can be involved in each of those.<sup>17,21,23</sup>

such as *Ala* and *Phe* was positively correlated to a successful crystallization outcome, while *Lys* and *Glu* negatively correlated.<sup>30</sup> Furthermore, it was verified that mean hydrophobicity promoted crystallization, while mean sidechain entropy, fractional positive or negative charge and disordered regions tended to hinder crystallization.<sup>30</sup> In terms of protein pI and chain length, both demonstrated bimodal effects, with the rate of success initially increasing and later decreasing with increasing parameter values. Examples of proteins that are easy targets for crystallization are soluble and globular proteins (e.g. lysozyme, insulin). Globular proteins consist of a hydrophobic core surrounded by a hydrophilic external surface which interacts with water (Fig. 3). In the specific case of lysozyme, the polar character of *Asp* and *Glu* residues is responsible for hydrogen bonding involved in crystal contacts.<sup>31</sup>

Overall, studies have suggested that crystal contacts correspond to non-randomly selected regions of the protein surface.<sup>10</sup> Therefore, it should be possible to control the protein–protein interactions involved in crystal contacts by tuning the solution conditions or by mutating certain surface residues.<sup>23</sup>

## 2.2. Protein solution quality

The purity, homogeneity, and stability of the protein solution considerably impact the likelihood of success in crystal formation.<sup>12</sup> There are plenty of possibilities concerning the assessment of the protein solution “quality”.<sup>32</sup> Herein, an overview of the most common techniques is presented (Table 1). Firstly, it is important to characterize the purity of the protein solution that should be as pure as possible (minimum of 90%). This is routinely achieved by sodium dodecyl sulfate polyacrylamide gel electrophoresis (SDS-PAGE), which separates proteins based on their molecular weight. Samples as low as 100 ng of protein can be detected



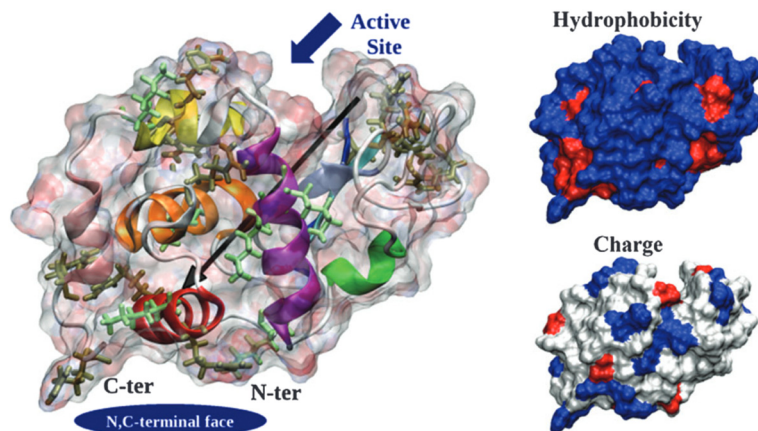


**Fig. 3** Hen egg-white lysozyme (HEWL) structure. Protein surface is shown as a ghost surface colored by partial charge with protein secondary structure elements indicated as a cartoon and colored: red –  $\alpha$ -helix A, orange –  $\alpha$ -helix B, purple –  $\alpha$ -helix C, yellow –  $\alpha$ -helix D, pink – C-terminal  $\alpha$ -helix  $3_{10}$  from domain  $\alpha$ , green – middle  $\alpha$ -helix  $3_{10}$  from domain  $\beta$ , blue – sheet  $\beta_1$ , cyan – sheet  $\beta_2$ , gray – sheet  $\beta_3$ , and white – other structures including loops, turns and  $\beta$ -bridges. *Arg* and *Lys* residues are shown as licorice and colored in tan and light green, respectively. The black arrow indicates the protein dipole moment. Protein termini, N,C-terminal face and active site location are shown by navy objects and annotated. Figures on the right-hand side show the distribution of charged (positive – blue, negative – red, and neutral – white) and hydrophilic (hydrophilic – blue and hydrophobic – red) residues. [Reproduced from ref. 24 with permission from The Royal Society of Chemistry].

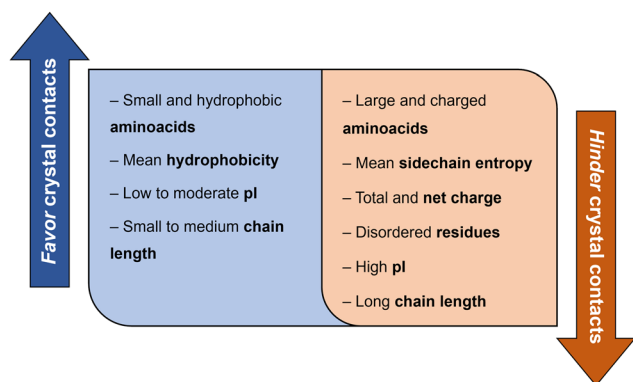


**Fig. 4** Correlation between protein surface properties favoring and hindering crystal contacts towards a successful crystallization trial.<sup>30</sup>

in a few hours.<sup>32</sup> Besides the purity of the protein solution, homogeneity and stability should also be checked. Dynamic light scattering (DLS) allows simultaneous determination of the monodispersity of the species of interest and the presence of soluble high-order assemblies and aggregates.<sup>33</sup> When performed over time and/or at different temperatures, the stability of the protein solution in different buffers can

also be tested. Likewise, the thermal stability of the protein in different buffers and in the presence of different ligands can be evaluated by differential scanning fluorometry (DSF).<sup>32</sup> In addition, information on parameters such as protein activity, integrity and folding can be used to assess the quality of the protein solution.<sup>32,34</sup> Activity assays are target-specific and have the additional benefit of measuring the fraction of active protein in a purified sample. Mass spectroscopy (MS) can be used to get detailed information about the protein primary structure, and thus on protein integrity.<sup>32</sup> Regarding protein folding, it can be checked by NMR spectroscopy.<sup>35</sup>

### 3. Measurement of the solubilized protein concentration in solution

Crystallization requires the creation of a supersaturated state for nucleation and subsequent protein crystal growth,<sup>36</sup> *i.e.* the quantity of the macromolecule present in solution must be higher than the solubility limit. The driving force of crystallization from solution ( $\Delta\mu$ ) arises thus from the difference between the chemical potential of the protein

**Table 1** Overview of the important steps in the assessment of protein solution quality

Analysis type	Measured parameter	First-line methods	Ref.
<b>Protein solution quality</b>	Purity	Separate and distinguish the protein of interest from other proteins ( <b>SDS-PAGE</b> )	32
	Homogeneity	Determine the monodispersity of the species of interest and the presence of aggregates ( <b>DLS</b> )	33
	Stability	Evaluate the stability over time ( <b>DLS</b> ) and the thermal stability ( <b>DFS</b> ) of the solution	32
<b>Additional analysis</b>	Activity	Measure the active and total concentration ( <b>UV-Vis spectroscopy</b> )	32
	Integrity	Analyze protein primary structure ( <b>MS</b> )	32
	Folding	Detect the folded and unfolded state ( <b>NMR</b> )	35



## Highlight

molecules in the supersaturated ( $\mu$ ) and saturated ( $\mu_s$ ) states as exhibited by eqn (1)<sup>36</sup>

$$\Delta\mu = \mu - \mu_s = R_g T (\ln a - \ln a_s), \quad (1)$$

where  $R_g$  is the gas constant, and  $T$  the absolute temperature.  $a$  and  $a_s$  are the protein activity in solution and the protein activity in solution in equilibrium with the crystals, respectively. Thus, this driving force can be expressed as a ratio of activities, which can be related to the concentration as defined by eqn (2)<sup>36</sup>

$$\frac{a}{a_s} = \frac{\gamma C}{\gamma_{\text{eq}} C_{\text{eq}}}, \quad (2)$$

where  $\gamma$  and  $\gamma_{\text{eq}}$  are the activity coefficient and activity coefficient at equilibrium, respectively.  $C$  is the molar protein concentration in solution, while  $C_{\text{eq}}$  is the molar protein concentration in solution at equilibrium (*i.e.* solubility). The ratio of activity coefficients in the supersaturated and saturated solutions ( $\gamma/\gamma_{\text{eq}}$ ) is often assumed to be equal to 1 ( $\gamma/\gamma_{\text{eq}} \approx 1$ ). Thereby, the driving force for crystallization can be expressed as the supersaturation ratio ( $S$ )<sup>36</sup>

$$S = \frac{C}{C_{\text{eq}}}. \quad (3)$$

Estimated values of supersaturation rely on the protein solubility and concentration measurements in solution. The main methods employed to measure protein solubility are presented in Table 3 and Fig. 5. Concerning the measurement of the protein concentration in solution, Table 2 compiles the principal methodologies used. UV-Vis spectroscopy at 280 nm is the most widely employed technique.<sup>32</sup> The method allows for direct measurement of protein concentration with no further reagents needed to be added and total recovery of the protein sample. However, its application is limited to cases where the extinction coefficient of the protein under study is known or calculated from its amino acid composition.<sup>37</sup> Additionally, the protein of interest must contain a known amount of tryptophans and tyrosines, since UV absorption at 280 nm is predominately from those aromatic amino acids.<sup>32,38</sup> Dye-binding assays such as biuret [*e.g.* bicinchoninic acid (BCA), Lowry],<sup>39</sup> colorimetric (*e.g.* Bradford),<sup>38</sup> and fluorescent<sup>40</sup> methods (Table 2) can be employed. Those assays involve the addition of a component that will directly or indirectly alter the color of the protein solution, whose intensity is proportional to the content of protein in the sample. Fourier transform infrared spectroscopy (FTIR)<sup>41</sup> is another technique that can be used to quantify protein concentration. From the FTIR spectrum, it is possible to determine the concentration of amine bonds from amide band I and II, and then calculate the protein concentration. Limitations include the equipment requisites (*e.g.* minimal and maximal concentrations) and the incompatibility of several amine-containing buffers (*e.g.* HEPES, Tris) or additives (*e.g.* EDTA).

## 4. Solubility measurement methodologies

Protein solubility is defined as the concentration of soluble protein that is in equilibrium with its crystal form under specific chemical and physical conditions (*e.g.* pH, temperature, additives).<sup>21</sup> In fact, it is crucial to establish reliable protein solubility data in each system to design crystallization assays. Trevino *et al.* (2008)<sup>48</sup> reviewed the different methodologies for measuring protein solubility, which include thermodynamic and apparent solubility experimentation. Thermodynamic solubility is defined as the concentration of soluble protein that is in equilibrium with a crystalline solid phase, while apparent solubility is defined as the concentration of soluble protein that is in equilibrium with an amorphous solid phase.

### 4.1. Thermodynamic solubility

Thermodynamic solubility is measured through equilibration of a protein solution with a crystalline solid phase<sup>42,48–58</sup> (Table 3 and Fig. 5). The solubility is then equal to the protein concentration in the equilibrated solution, which can be assayed by a suitable analytical technique (see Table 2). Two approaches have been used:<sup>48</sup> (1) dissolve crystals into an undersaturated solution until saturation is reached or (2) expose crystals to a supersaturated solution and allow crystal growth to bring the system to equilibrium (Fig. 5A). However, this methodology requires that crystallization conditions of the target protein must be known, and measurements can be laborious and time-consuming. Efforts have been made to reduce the required time and sample amount: Pusey & Gernert (1988)<sup>52</sup> and later Cacioppo *et al.* (1991)<sup>53</sup> developed a technique based upon maximization of the area for solute transfer, and minimization of the required solution volume to be brought to equilibrium. Nakazato *et al.* (2004)<sup>54</sup> observed concentration gradients around a lysozyme crystal *via* two-beam interferometry identifying dissolution or growth conditions. The authors derived the solubility curve of lysozyme in function of precipitant in two days using 7 mg of protein. More recently, Adawy *et al.* (2013)<sup>59</sup> employed phase shifting interferometry coupled to an image processing software program to study the concentration gradients developed around a lysozyme crystal during its growth and/or dissolution. Haire & Blow (2001)<sup>55</sup> reported the measurement of protein solubility through a spin filter method, where speed and simplicity of the method stand out, but around 20 mg of protein per filter is required.

Methodologies based on temperature variation<sup>42,60–62</sup> have also been described (Table 3 and Fig. 5B). They are based on the determination of the temperature at which a crystalline suspension becomes a clear solution during heating with a certain rate. Consequently, it consists in establishing “a clear point”, which can be determined by light scattering,<sup>61</sup> image analysis<sup>42,60,63</sup> or refractive index.<sup>62</sup>



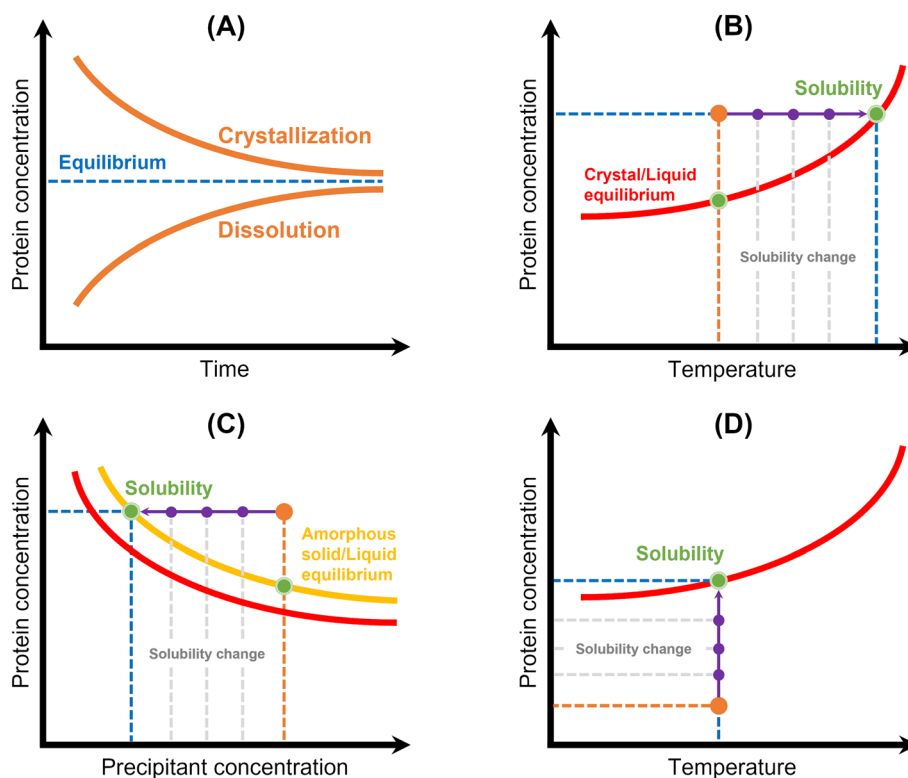


**Fig. 5** Schematic representation of the principles of the main methods used for protein solubility measurement: (A) equilibrium method, (B) temperature variation, (C) precipitation method, and (D) lyophilized protein addition and ultrafiltration/centrifugation. Red lines correspond to the crystal/liquid equilibrium curves, yellow line corresponds to the amorphous solid/liquid equilibrium curve, and protein concentration is represented in orange. Solubility is represented by a green spot, while solubility and/or protein concentration changes are represented by a purple arrow.<sup>12</sup>

Ferreira *et al.* (2020)<sup>60</sup> implemented an approach based on the temperature variation method to measure the solubility of lysozyme. First, the authors formed protein crystals in small crystallization drops by cooling. Then, temperature was increased, and an excess of saturated protein solution was added to the drop. Temperature was slowly increased until crystal dissolution was observed by optical microscopy. A similar methodology was employed by van Driessche *et al.* (2009).<sup>63</sup> The authors measured the *in situ* growth and dissolution of crystal surfaces with a laser confocal differential interference contrast microscope to determine the equilibrium temperature of glucose isomerase and lysozyme. In both cases,<sup>60,63</sup> equilibrium temperatures were determined within a short-range time and using a low amount of sample. However, this methodology is probably limited to model proteins (or well-known proteins), where it is necessary to know *a priori* the crystallization conditions and have some clues on the solubility of the system under study. Furthermore, the high costs and low accessibility of the instrumentation used in<sup>63</sup> as well as the expertise required to design a cell with high optical access and with only a few crystals should be noted. Feeling-Taylor *et al.* (1999)<sup>61</sup> reported a miniaturized optical scintillation technique ( $\sim 100 \mu\text{L}$ ), where temperature dependence of solubility for human hemoglobin was measured. Firstly, crystals are formed and detected by light scattering. Then, dissolution of the crystals is promoted by temperature increases.

#### 4.2. Apparent solubility

Owing to both the experimental time and the sample amount required to measure the thermodynamic solubility, more readily methods have been employed. Precipitation has been frequently used to measure protein solubility<sup>44,45,48,49,60,64–68</sup> (Table 3 and Fig. 5). This methodology consists in inducing protein precipitation through the addition of polymers (*e.g.* PEG) or salts (*e.g.* ammonium sulphate) and then measuring the concentration of protein in solution using an analytical technique (see Table 3) (Fig. 5C). Some studies reported turbidity measurements as a primary detection for the formation of a precipitate.<sup>66,67</sup> Precipitation allows faster solubility measurements, but only apparent solubility can be determined. The amorphous phase has different characteristics than the crystalline phase, and the control of the phase transition is rather difficult. For instance, protein solutions containing PEG can originate different protein phase behaviors (precipitates, crystals, or liquid–liquid phase separation) depending on the PEG concentration<sup>69</sup> (Fig. 5C). Liquid–liquid phase separation is commonly observed because of the high supersaturations required for crystallizing proteins.<sup>70</sup> Further, solubility values in the presence of an amorphous solid depend on the initial protein concentration, whereas solubility values in the presence of a crystalline solid phase do not.<sup>71</sup> In fact, it is known that amorphous solids are significantly more soluble than their



**Table 2** Main methodologies to measure the protein concentration in solution and respective studied proteins

Methodology	Advantages	Limitations	Studied protein	Ref.
<b>UV-Vis spectroscopy</b> Direct measurement of protein concentration	– Simple – Fast	– Depends on the composition of proteins' amino acids – Limited application	– BSA and IgG mAb – Insulin – Lysozyme	42 43 44–46 22*
<b>Biuret methods</b> Protein-copper chelation and secondary detection of reduced copper (BCA, Lowry)	– Compatibility with most surfactants – No dependency on the composition of amino acids of the protein	– Incompatibility with certain substances ( <i>e.g.</i> components that reduce copper, reducing agents)	– Serum total protein	39
<b>Colorimetric dye methods</b> Protein-dye binding and direct detection of the color change (Bradford)	– Fast – Compatibility with most components from the crystallization mixture	– Incompatibility with surfactants – Dependency on the composition of amino acids	– BSA and IgG mAb – Insulin – Ref2NM, MAGOH, WW34, Y14, OFR57, and TAP	38 43 47
<b>Fluorescence dye methods</b> Protein-dye binding and direct detection of increase in fluorescence associated with the bound dye	– High sensitivity	– Specialized equipment – Low compatibility with certain components from the crystallization mixture ( <i>e.g.</i> detergents, solvent)	– Proteins from tissue lysates	40
<b>FTIR</b> Determination of the concentration of amine bonds	– No dependency on the composition of amino acids of the protein	– Equipment specificities – Incompatibility with buffers and additive containing amine	– Proteins from raw milk	41

**Note:** \*the referred paper is a review.

crystalline counterparts.<sup>72</sup> Ferreira *et al.* (2020)<sup>60</sup> used both precipitation and crystallization methods to measure lysozyme solubility and verified significant differences. The authors mentioned that structurally different lysozyme aggregates were probably produced during precipitation. Hofmann *et al.* (2018)<sup>65</sup> verified that PEG-induced precipitation was not adequate to predict the solubility of a single-domain antibody construct. Possible explanations included conformational changes of the protein, volume exclusion effects of PEG and high protein concentration, which led to specific protein phase behavior when compared to diluted protein solutions.

The addition of lyophilized protein to solvent and concentration of a protein solution by ultrafiltration have also been employed<sup>48,68</sup> (Table 3 and Fig. 5). Both methods require that the concentration of protein in solution be increased until saturation is reached (Fig. 5D). However, it can be difficult to carry out with highly soluble proteins, once gel-like or supersaturated solutions may form,<sup>68</sup> hampering the determination of solubility accurately. In addition, lyophilized protein contains additional components such as water and salt, which can significantly impact solubility measurement.<sup>73,74</sup>

## 5. Measurement of other thermodynamic parameters that quantify protein binding

The second virial coefficient ( $B_{22}$ ), enthalpy ( $\Delta H$ ), and entropy ( $\Delta S$ ) are thermodynamic parameters enabling the measurement of the binding ability of a given protein in solution. Protein interactions are typically expressed in terms of the second virial coefficient,<sup>80</sup> while the

measurement of enthalpy and entropy changes provides a quantitative description of the forces governing molecular associations.<sup>81</sup>

### 5.1. Protein-protein interaction measurement – second virial coefficient

The second virial coefficient ( $B_{22}$ ) provides a measure of the protein-protein interactions, including contributions from excluded volume, electrostatic factors (attractive and repulsive) and hydrophobic interactions, which has been extensively reviewed by Wilson & Delucas (2014).<sup>80</sup> For relatively weak interactions,  $B_{22}$  quantifies the deviation of a dilute solution from thermodynamic ideality. Thus, the osmotic virial coefficient ( $\Pi$ ) can be defined by eqn (4)<sup>82,83</sup>

$$\Pi = R_g T C_p \left( \frac{1}{M_w} + B_{22} C_p + \dots \right), \quad (4)$$

where  $C_p$  is the protein mass concentration and  $M_w$  the protein molecular weight. Considering protein molecules as spheres, the second virial coefficient can be expressed by eqn (5)<sup>82,83</sup>

$$B_{22} = -\frac{2\pi}{M_w^2} \int_0^\infty \left[ \exp\left(-\frac{W}{k_B T}\right) - 1 \right] r^2 dr, \quad (5)$$

where  $W$  is the potential mean force and  $k_B$  the Boltzmann constant, while  $r$  corresponds to the radial direction.  $B_{22}$  reflects the deviation degree of the osmotic pressure of a protein solution from an ideal solution, *i.e.* when  $B_{22} = 0$ . Therefore, positive and negative values of  $B_{22}$  indicate predominantly repulsive and attractive interactions, respectively. Following this approach, the determination of  $B_{22}$  can be useful for the selection of solution conditions favorable for protein







interactions. Besides this aspect, multicomponent solutions are usually used to crystallize proteins, where the contribution of the interactions between protein and salt or polymers must be considered. On the other hand, the formation of a crystal requires protein–protein contacts that are correctly positioned to form an ordered crystalline lattice, and those contacts do not occur randomly but require selection of the binding partner.<sup>30,42</sup> Constraints related to the measurement of  $B_{22}$  by SLS, such as the protein amount and time required, as well as the challenges associated with multicomponent systems, led to the exploration of other techniques.<sup>80,88</sup>

SIC is based on the assumption that increased attraction between the injected mobile-phase protein and the covalently, but randomly bound protein will result in an increase in the solution volume required to elute the injected protein from the column<sup>80,88,96,97</sup> (Table 4). Valente *et al.* (2005)<sup>97</sup> demonstrated that SIC provides a valid approach to measure  $B_{22}$  for lysozyme self-interaction as a function of several cosolvents. Tessier *et al.* (2003)<sup>96</sup> verified a quantitative agreement between  $B_{22}$  measured by SIC and SLS for both lysozyme and chymotrypsinogen over a wide range of pH and ionic strengths. Nevertheless, experimental concerns can be related to the need for protein immobilization, and the fact that the impurities/additives present in solution may bind the immobilized protein sites.

Ruppert *et al.* (2001)<sup>84</sup> derived an empirical relation between  $B_{22}$  and solubility. The authors verified a good agreement between the model and the experimental data for different experimental conditions (*i.e.* protein type and concentration, salt type and concentration, temperature, and pH) for the low-solubility range (up to 30 mg mL<sup>-1</sup>). A correlation between  $B_{22}$  and solubility was also observed by

Guo *et al.* (1999)<sup>86</sup> for lysozyme and ovalbumin under various solvent conditions. More recently, Link & Heng (2022)<sup>76</sup> observed a 5-fold increase in insulin solubility with pH increase from 6.0 to 6.7, but SLS measurements showed no significant alteration of  $B_{22}$ . Both  $B_{22}$  and solubility are strongly affected by solution parameters such as pH and ionic strength, or precipitating type/concentration, which could explain such differences.

## 5.2. Thermodynamic definition – Gibbs free energy

The change in Gibbs free energy ( $\Delta G$ ) depends on the enthalpic ( $\Delta H$ ) and entropic ( $\Delta S$ ) contributions as defined by eqn (6)<sup>81</sup>

$$\Delta G = \Delta H - T\Delta S, \quad (6)$$

where  $\Delta H$  can be regarded as a reflection of the nature of intermolecular contacts and hydration, while  $\Delta S$  is related to the change in the number of possible conformations of a molecule.<sup>98</sup>  $\Delta H$  has mostly been assessed indirectly from solubility data (*indirect methods*) but it can be directly measured by microcalorimetry (*direct methods*). Regarding  $\Delta S$ , it can only be determined indirectly from solubility data (*indirect methods*).<sup>81</sup>

**5.2.1. Direct methods.** During a first-order phase transition, a thermodynamic system releases or absorbs latent heat and crystallization is not an exception. Upon protein crystallization, the binding energy of the protein molecules is released as heat.<sup>81</sup> The exothermal signal of the crystallizing protein solution can be recorded from calorimetry experiments to experimentally determine the crystallization enthalpy ( $\Delta H$ ).<sup>81</sup> This methodology is

**Table 4** Main equations and techniques to experimentally determine  $B_{22}$  and the respective studied proteins

Technique	Equations & techniques	Advantages	Limitations	Studied protein	Ref.
<b>SLS</b>	$B_{22} = \frac{1}{2C_p} \left( \frac{K_c C_p}{R_\theta} - \frac{1}{M_w} \right)$ where $K_c = \frac{4\pi n^2 \left( \frac{dn}{dc_p} \right)^2}{N_A \lambda^4}$	– Diagnostic of solution conditions that lead to crystallization	– Protein amount and time required – High sensitivity to the presence of aggregates – Low compatibility with multicomponent mixtures	– Equine serum albumin and thaumatin – Insulin – Lysozyme – mAb anti-CD20	87 76 87 and 94 83 and 95
<b>SIC</b>	$B_{22} = \left( \frac{N_A}{M_w} \right) \left( B_{HS} - \frac{k'}{\phi \rho} \right)$ where $k' = \frac{V_r - V_0}{V_0}$	– High sensitivity – High compatibility with multicomponent mixtures – Possibility of automation and miniaturization	– Protein immobilization required – Impurities/additives may interfere with protein binding sites	– Catalase, concanavalin A, and lactoferrin – Lysozyme	88 88 and 97 80 and 96*
<b>Other techniques</b>	– Size exclusion chromatography (SEC)			– Lysozyme	84, 89, 91 and 92
	– Membrane osmometry (MO)			– mAbs	80 and 90–92
	– Sedimentation velocity analytical ultracentrifugation (SV-AUC)			– Ovalbumin	84

**Notes:** \*the referred papers are reviews.  $K_c$  is the optical constant,  $R_\theta$  the excess Rayleigh ratio at scattering angle  $\theta$ ,  $(dn/dc_p)$  the refractive index increment for the protein/solvent pair,  $n$  the refractive index of the solvent,  $N_A$  the Avogadro's number, and  $\lambda$  the wavelength of the laser beam.  $B_{HS}$  is the protein excluded volume,  $k'$  the chromatographic capacity factor,  $\phi$  the surface area of the protein-modified particles that is available to the mobile phase protein,  $\rho$  the number of covalently immobilized protein molecules per unit of surface area of the bare chromatography particles,  $V_r$  the volume required to elute the interacting mobile phase protein, and  $V_0$  the volume required to elute a non-interacting species (neutral marker) of equivalent size.



combined with spectrophotometric measurement of protein concentration in solution to assess the fraction of crystallized protein ( $\Delta C_p V$ ) (Table 5). There are few reports on the measurement of  $\Delta H$  due to experimental difficulties. For instance, it is important to ensure that the onset and offset of the crystallization process is neither too fast compared to the initial thermalization of the sample and instrument nor too slow to allow for a significant signal. Besides, the value of  $\Delta H$  is typically less than  $100 \text{ kJ mol}^{-1}$ ,<sup>43,81,99</sup> which is difficult to measure. Recently, Hentschel *et al.* (2021)<sup>81</sup> measured the  $\Delta H$  of lysozyme solutions by combining microcalorimetry with UV-Vis spectroscopy. The authors verified that the measured values agree with the ones determined by the van 't Hoff equation based on solubility data.

**5.2.2. Indirect methods.**  $\Delta H$  and  $\Delta S$  can be determined indirectly based on the van 't Hoff analysis of solubility data<sup>81</sup> (Table 5). For simplicity, the relationship between the equilibrium constant and temperature can be represented by the van 't Hoff equation, which is derived from the relationship between equilibrium constants and Gibbs free energy as expressed by eqn (7)<sup>43,81,98</sup>

$$\ln K = -\frac{\Delta G}{R_g T}, \quad (7)$$

where  $K$  is the equilibrium constant, which can be represented by eqn (8)<sup>37,73</sup>

$$K = \frac{1}{a_{\text{eq}}} = \frac{1}{\gamma_{\text{eq}} C_{\text{eq}}}, \quad (8)$$

where  $C^0$  is the molar protein concentration in a hypothetical solution standard state (1 M). By combining eqn (7) and (8) and assuming a solution close to ideality ( $\gamma_{\text{eq}} \approx 1$ ), eqn (9) can be derived

$$\Delta G = -R_g T \ln a_{\text{eq}} \cong R_g T \ln \left( \frac{C_{\text{eq}}}{C^0} \right). \quad (9)$$

## 6. Instrumentation for solubility measurements

After revising the employed methodologies and techniques for protein solubility measurements, this section introduces the platforms and protocols that are currently available in the literature for this purpose. In fact, the reported literature is especially focused on APIs (active pharmaceutical ingredients) (*e.g.* paracetamol, adipic acid). However, the increasing interest in proteins has contributed to the appearance of several protein-oriented devices. Stura *et al.* (1992)<sup>101</sup> designed a simple standard screen (*footprint*) for the comparison of protein solubilities, which was aided by SDS-PAGE and isoelectric focusing data to monitor and relate crystallization results to biochemical analysis. This screening strategy revealed a high success rate in crystal production for both proteins (*e.g.* glycoproteins) and more complex biological systems. The set-up consisted of a temperature controlled multiwell sitting-drop vapor diffusion tray. Later, Santesson *et al.* (2003)<sup>64</sup> followed the *Stura footprinting* screening strategy for D-serine dehydratase.

### 6.1. Thermodynamic solubility experimentation

During the last decades, several protocols were reported in the literature by covering distinct protocols and set-ups. Pusey & Gernert (1988)<sup>52</sup> developed a column packed with protein microcrystals, which was fed by a solution below and above the solubility limit to enable dissolution or crystal growth, respectively. The authors were able to measure lysozyme

**Table 5** Methods to determine enthalpic variables ( $\Delta H$  and  $\Delta S$ ) and the respective studied proteins

	Technique	Equation	Studied protein & thermodynamic values	Ref.
<b>Direct</b>	<b>Calorimetry</b>	$Q = \int_{t_i}^{t_f} \Delta P(t) dt$ $\Delta H = \frac{M_w}{\Delta C_p V} Q$	- Lysozyme $\Delta H \approx 65 \text{ kJ mol}^{-1}$	81
<b>Indirect</b>	<b>van't Hoff analysis of solubility data</b>	$\Delta H = T\Delta S - R_g T \ln \left( \frac{C_{\text{eq}}}{C^0} \right)$	- Chymotrypsinogen A $\Delta H \in [-79.8, -27.2] \text{ kJ mol}^{-1}$	90
			- Glucose isomerase $\Delta H \in [-174, -144] \text{ kJ mol}^{-1}$ $\Delta S \in [-462, -370] \text{ J mol}^{-1} \text{ K}^{-1}$	63
			- Hemoglobin $\Delta H = 155 \text{ kJ mol}^{-1}$	61
			- Insulin $\Delta H \in [-55, -20] \text{ kJ mol}^{-1}$ $\Delta S \in [-110, -35] \text{ J mol}^{-1} \text{ K}^{-1}$	43
			- Orthorhombic lysozyme $\Delta H = 22 \text{ kJ mol}^{-1}$	45
			- Tetragonal lysozyme $\Delta H \in [-129, -31] \text{ kJ mol}^{-1}$ $\Delta S \in [-10, 241] \text{ J mol}^{-1} \text{ K}^{-1}$	45, 63, 81, 90, 93 and 100

**Note:**  $Q$  is the heat released upon crystallization,  $\Delta P$  the differential microcalorimetric power signal,  $V$  the sample volume, and  $t_i$  and  $t_f$  the initial and final times, respectively.



## Highlight

solubility within a time frame of 24 h using a column volume between 1 and 5 mL. Later, the methodology was improved by Cacioppo *et al.* (1991),<sup>53</sup> where the required column volume was reduced to a range between 75 and 900  $\mu\text{L}$ .

Haire & Blow (2002)<sup>55</sup> used a spin filter method to measure protein solubility. It consisted of equilibrating a crystal slurry with protein solution and then centrifuging through a filter to assay the protein concentration. More recently, Nakazato *et al.* (2004)<sup>54</sup> developed a dialysis cell for both direct optical measurement of protein concentration and observation of concentration gradients around a crystal *via* two-beam interferometry. Chen *et al.* (2005)<sup>57</sup> reported one of the first droplet-based microfluidic devices for crystallizing proteins. However, the authors measured the solubility of thaumatin in Eppendorf tubes by both dissolution of protein crystals and crystallization of thaumatin solution. Table 6 summarizes the reported works where thermodynamic solubility experiments were performed.

### 6.2. Apparent solubility experimentation

Guilloteau *et al.* (1992)<sup>44</sup> revealed that information about solubility data allows the determination of optimum supersaturation conditions, thus contributing to a better experimental reproducibility. Moreover, the authors concluded that the temperature influence on the protein (lysozyme) solubility and crystal form was modulated by the salt nature. Table 7 summarizes the reported works where apparent solubility experiments were performed.

### 6.3. Solubility screening in microfluidic devices

The conventional protein crystallization techniques such as vapor diffusion (hanging-drop or sitting-drop), microbatch, *etc.* rely on testing many potential crystallization conditions, while consuming large amounts of the protein of interest, without any theoretical background guidance. Therefore, microfluidic devices constitute a high-throughput methodology to systematically screen crystallization conditions and, simultaneously, limit the protein volume consumption. Moreover, microfluidics allows complex protocols to be carried out on a single chip (Lab-on-a-Chip devices) for fluid-handling and processing. These devices offer attractive advantages over conventional macroscale instruments, such as shorter operation times, higher mixing and heat transfer efficiencies, lower energy consumption, *etc.*<sup>102,103</sup> Sommer & Larsen (2005)<sup>104</sup> highlighted that the developed protocol based on tailor-made microbatch crystallization screening resulted in around 50% crystallization probability per experiment for the studied proteins (SERCA and UMP kinase). Most of the reported works in microfluidic devices consist in implementing the microbatch technique, but this is not the only implemented traditional crystallization technique. Leng & Salmon (2009)<sup>13</sup> revised the existent microfluidic devices for crystallization applications more focused on lab-on-a-chip instrumentation for protein crystallization condition screening. More recently, Candoni *et al.* (2019)<sup>105</sup> published a review paper highlighting

microfluidic devices developed by the research team for solubility and crystallization experimentation, mostly covering APIs (*e.g.* paracetamol, sulfathiazole, glyclazide) and a few protein examples (*e.g.* lysozyme, rasburicase, QR2). Microfluidic devices were also applied for measuring thermodynamic parameters as reported elsewhere.<sup>100,106,107</sup> Table 8 and Fig. 6 present an overview of the reported microfluidic devices used to screen protein solubility conditions.

## Outlook and future perspectives

This highlight critically reviews the advances in experimental approaches to measure thermodynamic parameters able to assess protein solubility and, consequently, to enhance crystal formation propensity. Initially, protein interactions and protein solution quality are highlighted as the main variables to successfully crystallize a protein, which reveals the importance of being characterized before conducting any assay. Secondly, within the methodologies to measure protein solubilities (thermodynamic and apparent), efforts have been directed towards the reduction of the required sample amount and time. In what concerns the assessment of intermolecular interactions, discrepancies between second virial coefficient measurements and protein aggregation rates have been frequently observed. Lastly, experimental protocols and platforms are revised in terms of apparatus capabilities, experimental techniques, and studied proteins. Microfluidic devices offer unequalled conditions to conduct protein solubility experiments and are capable of answering both questions: sample amount and time.

Despite the significant developments in this research field, there is still room for improvement. In this context, one can learn from the strategies applied to small organic molecules (*e.g.* APIs), even though protein and small organic molecules have distinct behaviors. Traditional and advanced procedures and instrumentation commonly used to measure small organic molecules' solubility can be adapted to experimentally determine protein solubility. The solvent addition method consists in adding a solvent dropwise, at a constant temperature, to a known crystalline suspension until full dissolution of the material is observed. Reus *et al.* (2015)<sup>110</sup> applied the solvent addition method in a multi-reactor crystallizer (*Crystal16*) for the measurement of *p*-hydroxybenzoic acid solubility. The authors determined a "clear point" through turbidity measurements, video recording, and FTIR concentration measurements. The results showed that the obtained solubility values agreed with the equilibrium method. This could represent an alternative to the equilibrium method as it enables more expeditious solubility measurements. Nevertheless, crystallization conditions of the protein under study must be known, and operating parameters such as the required volume and accuracy of the detection technique must be considered. Another important aspect to mention is the equipment used, *Crystal16*. It is a well-known commercialized apparatus to measure, not only the solubility, but also to screen a phase



**Table 6** Summary of the reported experimental protocols and respective platforms for thermodynamic solubility experimentation and studied proteins

Apparatus capabilities and associated techniques	Solubility screening details	Studied protein	Ref.
<ul style="list-style-type: none"> <li>– Eppendorf tubes at fixed temperature</li> <li>– Frequent gentle mixing procedure</li> <li>– Nanodrop UV-Vis spectrophotometer for protein concentration measurements</li> </ul>	<ul style="list-style-type: none"> <li>– Increase in solubility as a function of pH</li> <li>– Solubility independency of the zinc salt type</li> </ul>	– Insulin	76
<ul style="list-style-type: none"> <li>– Temperature-controlled vials</li> <li>– HPLC analysis for protein concentration measurements</li> </ul>	<ul style="list-style-type: none"> <li>– Amino acids increase solubility (arginine)</li> <li>– Amino acids do not alter solubility (leucine and glycine)</li> </ul>	– Insulin	75
<ul style="list-style-type: none"> <li>– Set-up consists of drop jacketed glass cell</li> <li>– UV-Vis spectrophotometer for protein concentration measurements</li> </ul>	<ul style="list-style-type: none"> <li>– Polymeric additives induce entropic variations while the structural integrity is preserved</li> <li>– Enthalpic variations induced by pH and ionic strength</li> <li>– Enhanced chemical activity evidenced by lower solubility values</li> </ul>	– Lysozyme	60
<ul style="list-style-type: none"> <li>– Novel approach using laser confocal differential interference contrast microscopy (LCM-DIM) in a temperature-controlled stage</li> </ul>	<ul style="list-style-type: none"> <li>– Fast and precise determination of solubility in function of temperature</li> <li>– Determination of thermodynamic parameters (enthalpy and entropy)</li> <li>– Derivation of solubility curves</li> </ul>	<ul style="list-style-type: none"> <li>– Glucose isomerase</li> <li>– Lysozyme</li> </ul>	63
<ul style="list-style-type: none"> <li>– Microdialysis crystallization method</li> <li>– Crystal quality characterized by the Wilson plot method</li> </ul>	<ul style="list-style-type: none"> <li>– Determination of solubility curves at variable pH and precipitation solution concentration ranges</li> <li>– Crystal quality influenced by pH</li> </ul>	– Lysozyme	56
<ul style="list-style-type: none"> <li>– Eppendorf tubes at fixed temperature</li> <li>– UV-Vis spectrophotometer for protein concentration measurements</li> </ul>	<ul style="list-style-type: none"> <li>– Significant solubility differences under different precipitant solutions</li> </ul>	– Thaumatin	57
<ul style="list-style-type: none"> <li>– Batch technique with temperature-controlled vials</li> <li>– UV-Vis spectrophotometer and Bradford reagent for protein concentration measurements</li> </ul>	<ul style="list-style-type: none"> <li>– Temperature, and enthalpy and entropy dependence of solubility at varying solution composition and temperature</li> </ul>	– Insulin	43
<ul style="list-style-type: none"> <li>– Automated microbatch method for initial screening</li> <li>– Hanging-drop vapor diffusion set-up</li> <li>– Decoupling nucleation and growth stages</li> </ul>	<ul style="list-style-type: none"> <li>– Derivation of solubility curves</li> </ul>	<ul style="list-style-type: none"> <li>– Trypsin</li> <li>– C-Phycocyanin</li> </ul>	15
<ul style="list-style-type: none"> <li>– Miniature column solubility apparatus</li> <li>– Recrystallization and redissolution by dialysis</li> <li>– SDS-PAGE for protein species identification</li> </ul>	<ul style="list-style-type: none"> <li>– Wide range of temperature, pH, and sodium chloride solution concentration</li> <li>– Rapid determination of solubility curves</li> <li>– Solubility increases in function of temperature</li> <li>– pH has a varied and unpredictable effect on solubility</li> </ul>	– Lysozyme	46
<ul style="list-style-type: none"> <li>– Miniaturized scintillation arrangement with integrated temperature control</li> <li>– X-ray crystallography for structural characterization</li> </ul>	<ul style="list-style-type: none"> <li>– Determination of solubility in function of temperature</li> <li>– Estimation of thermodynamic parameters (enthalpy)</li> </ul>	– Hemoglobin	61
<ul style="list-style-type: none"> <li>– Novel technique consisting of a Michelson interferometer and a temperature controlled-stage</li> <li>– High accuracy and time saving protocol</li> </ul>	<ul style="list-style-type: none"> <li>– Applicable to solubility measurements of a metastable phase</li> <li>– Solubility curves for tetragonal and orthorhombic crystal forms</li> </ul>	– Lysozyme	77
<ul style="list-style-type: none"> <li>– Batch set-up</li> <li>– Hanging-drop vapor diffusion set-up</li> <li>– Diffractometer for crystal lattices characterization</li> </ul>	<ul style="list-style-type: none"> <li>– Slight solubility differences in H<sub>2</sub>O and D<sub>2</sub>O, possibly because of differences between H and D bonds</li> </ul>	– Lysozyme	58
<ul style="list-style-type: none"> <li>– Easy to use semi-micro column apparatus</li> <li>– Optimized set-up configuration</li> <li>– Eliminates the time factor when deriving protein phase diagrams</li> </ul>	<ul style="list-style-type: none"> <li>– Rapid determination of solubility curves</li> <li>– Solubility increase of different crystal forms with decreasing salt concentration and increasing temperature</li> </ul>	– Lysozyme	53



Table 6 (continued)

Apparatus capabilities and associated techniques	Solubility screening details	Studied protein	Ref.
<ul style="list-style-type: none"> <li>- Automated microbatch system</li> <li>- Complete sample mixing</li> <li>- Minimal evaporation</li> <li>- Application specific software</li> <li>- Low operation cost</li> </ul>	<ul style="list-style-type: none"> <li>- Speed and ease of operation, and simplicity</li> <li>- Determination of broad protein solubility properties</li> </ul>	<ul style="list-style-type: none"> <li>- Lysozyme</li> <li>- Glucose isomerase</li> <li>- ETI</li> </ul>	49

Table 7 Summary of the reported experimental protocols and respective platforms for apparent solubility experimentation and studied proteins

Apparatus capabilities and associated techniques	Solubility screening details	Studied protein	Ref.
<ul style="list-style-type: none"> <li>- Set-up consists of drop jacketed glass cell</li> <li>- UV-Vis spectrophotometer for protein concentration measurements</li> </ul>	<ul style="list-style-type: none"> <li>- Polymeric additives induce entropic variations while the structural integrity is preserved</li> <li>- Enthalpic variations induced by pH and ionic strength</li> <li>- Enhanced chemical activity evidenced by lower solubility values</li> </ul>	<ul style="list-style-type: none"> <li>- Lysozyme</li> </ul>	60
<ul style="list-style-type: none"> <li>- <i>In-house</i> acoustically levitated drops set-up</li> <li>- Commercial kits from Hampton research in standard vapor diffusion experiments for crystallization trials</li> <li>- Right-angle light scattering for protein concentration measurements</li> </ul>	<ul style="list-style-type: none"> <li>- Several crystallizing agents are tested</li> <li>- Concentration measurements of all components in the drop at any time during the experiment</li> <li>- Derivation of solubility curves followed by crystallization condition optimization</li> </ul>	<ul style="list-style-type: none"> <li>- Alcohol dehydrogenase</li> <li>- D-Serine dehydratase</li> </ul>	64
<ul style="list-style-type: none"> <li>- Thermal denaturation experiments performed on AVIV spectrophotometers</li> </ul>	<ul style="list-style-type: none"> <li>- Increased negative surface charge strongly correlates with increased solubility</li> <li>- No correlation between positive surface charge and solubility</li> </ul>	<ul style="list-style-type: none"> <li>- <math>\alpha</math>-Chymotrypsin</li> <li>- Lysozyme</li> <li>- Serum albumin</li> <li>- RNase Sa</li> <li>- Ovalbumin</li> <li>- <math>\alpha</math>-Lactalbumin</li> <li>- Fibrinogen</li> </ul>	68
<ul style="list-style-type: none"> <li>- Novel method using a high-throughput screening approach (robotic liquid handling section)</li> <li>- Photometric turbidity measurements and <i>in-line</i> concentration measurements</li> <li>- Controlled concentration of the solution while constantly analyzing the solution state</li> </ul>	<ul style="list-style-type: none"> <li>- Determination of process relevant solubility limits</li> <li>- Analysis of relevant kinetic effects (buffer systems)</li> </ul>	<ul style="list-style-type: none"> <li>- Lysozyme</li> <li>- Insulin</li> </ul>	78
<ul style="list-style-type: none"> <li>- UV-Vis spectrophotometer for protein concentration measurements</li> <li>- Diffractometer for crystal lattice characterization</li> </ul>	<ul style="list-style-type: none"> <li>- Solubility curve measurements</li> <li>- Slight influence of the cation nature on the solubility</li> <li>- Solubility and crystal form are affected differently by temperature changes</li> <li>- Salt nature determines the crystal form</li> </ul>	<ul style="list-style-type: none"> <li>- Lysozyme</li> </ul>	44
<ul style="list-style-type: none"> <li>- Automated microbatch system</li> <li>- Complete sample mixing</li> <li>- Minimal evaporation</li> <li>- Application specific software</li> <li>- Low operation cost</li> </ul>	<ul style="list-style-type: none"> <li>- Speed and ease of operation, and simplicity</li> <li>- Determination of broad solubility properties</li> </ul>	<ul style="list-style-type: none"> <li>- Lysozyme</li> <li>- Glucose isomerase</li> <li>- ETI</li> </ul>	49
<ul style="list-style-type: none"> <li>- Batch set-up in polystyrene test tubes</li> <li>- Ultrafiltration crystallization method at controlled temperature</li> <li>- UV-Vis spectrophotometer for protein concentration measurements</li> </ul>	<ul style="list-style-type: none"> <li>- Solubility examined as a function of temperature, pH, and salt concentration</li> <li>- Negative crystallization enthalpy for tetragonal crystal form</li> <li>- Positive crystallization enthalpy for orthorhombic crystal form</li> </ul>	<ul style="list-style-type: none"> <li>- Lysozyme</li> </ul>	45

diagram. The system consists of a micro-vial set-up with an integrated transmissivity technology from *Technobis Crystallization Systems*.<sup>111</sup> The theoretical understanding behind the equipment was initially introduced by ter Hoort's

group.<sup>112</sup> More recently, Peybernès *et al.* (2018)<sup>73</sup> performed *in situ* solubility measurements of organic compounds directly from powder using small amounts of material (30 mg) and a time frame of a few hours. The authors



**Table 8** Summary of the reported microfluidic devices for protein solubility screening and respective studied proteins

Crystallization technique	Device capabilities	Solubility screening details	Studied protein	Ref.
<b>Microbatch</b>	<ul style="list-style-type: none"> <li>– Versatility aspect: on-chip dialysis and <i>in situ</i> X-ray diffraction</li> <li>– Screening and optimization through concentration and temperature control</li> <li>– Tailoring crystal size, number, and quality</li> </ul>	<ul style="list-style-type: none"> <li>– Micro-dialysis method</li> <li>– Crystallization and dissolution experiments based on phase behaviors</li> </ul>	<ul style="list-style-type: none"> <li>– Lysozyme</li> <li>– Insulin</li> <li>– IspE</li> </ul>	108
<b>Microbatch (dispersed microdroplets)</b>	<ul style="list-style-type: none"> <li>– Chemical library for non-specialists in microfluidics</li> <li>– Screening and optimization through concentration and temperature control</li> <li>– Concentration measurements <i>via in-line</i> UV-Vis</li> <li>– Crystals characterization <i>via</i> X-ray diffraction</li> </ul>	<ul style="list-style-type: none"> <li>– Directly solubilizing powder (only for APIs)</li> <li>– Derivation of solubility curves</li> </ul>	<ul style="list-style-type: none"> <li>– Lysozyme</li> <li>– Rasburicase</li> <li>– QR2</li> <li>– <i>etc.</i></li> </ul>	105
<b>Reverse vapor diffusion</b>	<ul style="list-style-type: none"> <li>– Drop state is determined at any point in time</li> <li>– Efficient method to traverse phase space along a known path in the phase diagram</li> <li>– Possibility to decouple nucleation and growth events to enhance crystal size and quality</li> </ul>	<ul style="list-style-type: none"> <li>– Evaporation-based method</li> <li>– Determination of solubility boundaries</li> </ul>	<ul style="list-style-type: none"> <li>– Lysozyme</li> <li>– Ribonuclease A</li> <li>– bacteriorhodopsin</li> </ul>	50
<b>Microbatch</b>	<ul style="list-style-type: none"> <li>– Tailor-made crystallization screening</li> <li>– High probability of yielding crystallization hits</li> </ul>	<ul style="list-style-type: none"> <li>– Complete screening of phase behaviors</li> </ul>	<ul style="list-style-type: none"> <li>– SERCA</li> <li>– UMP kinase</li> </ul>	104
<b>Microbatch</b>	<ul style="list-style-type: none"> <li>– Fully automated</li> <li>– Formulation chip: rapidly generation of complex mixtures</li> <li>– Design of maximum likelihood crystallization trials</li> </ul>	<ul style="list-style-type: none"> <li>– Complete mapping of phase behaviors</li> </ul>	<ul style="list-style-type: none"> <li>– Lysozyme</li> <li>– Xylanase</li> </ul>	109

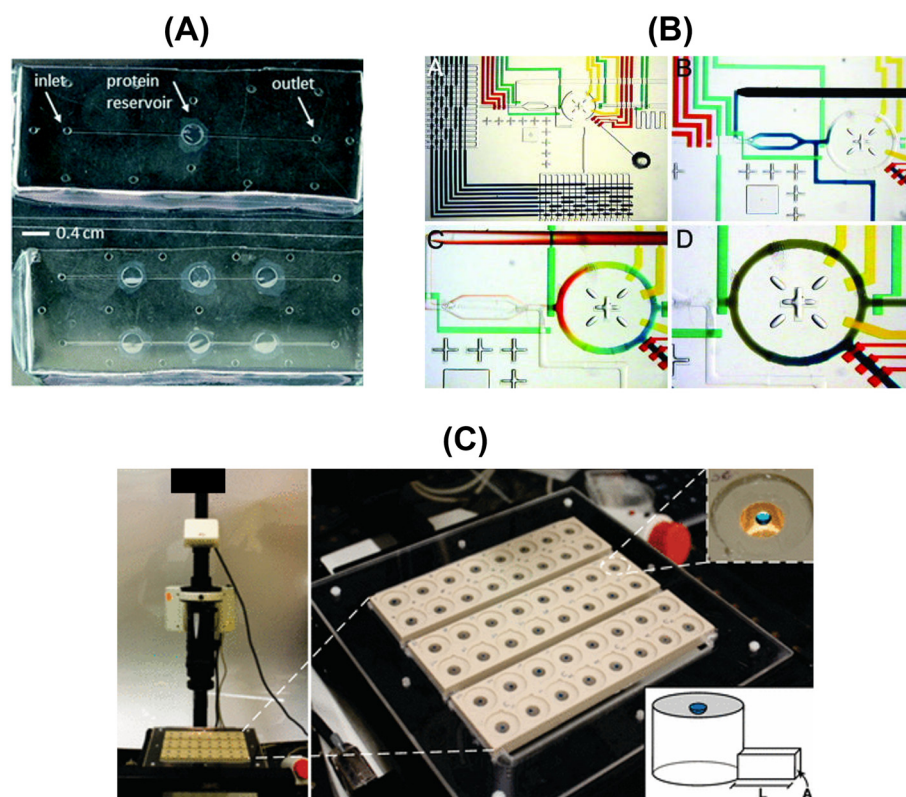


**Fig. 6** Overview of the designed and fabricated microfluidic platforms for protein solubility measurements: (A) top-view of the microfluidic chips embedding the dialysis membrane for the on-chip crystallization of proteins and *in situ* X-ray measurements [adapted from ref. 108 with permission from The Royal Society of Chemistry], (B) optical micrographs showing the combinatorial mixing using a microfluidic formulator. [Adapted from ref. 109 with permission from the Proceedings of the National Academy of Sciences of the United States of America (copyright (2004) National Academy of Sciences, U.S.A.)], and (C) photograph of the automated data acquisition set-up: three 16-compartment evaporation-based crystallization platforms [adapted from ref. 50 (<https://pubs.acs.org/doi/full/10.1021/jp911780z>)]. Further permission related to the material excerpted should be directed to the American Chemical Society].



## Highlight

developed a microfluidic set-up where the solvent flows through the powder bed blocked by a filter. At the outlet of the filter, due to the dissolution of the powder, the solution is saturated.

Regardless of all the experimental advances and employed methodologies and platforms, the task of measuring protein solubility can still be a costly and time-consuming process, frequently characterized by low success rates. Furthermore, the methods described along the highlight are often not readily amenable for high-throughput screening. Therefore, sequence-based computational tools have been used to predict protein solubility.<sup>113,114</sup> However, these tools suffer from relatively low prediction accuracy and limited applicability for various classes of proteins, mostly only covering model proteins (e.g. lysozyme, thaumatin, insulin). Accuracy can be improved by using more advanced algorithms and incorporating additional information. For instance, protein 3D structure information can be used to provide more geometric information of each amino acid residual.<sup>115</sup> It is also worth mentioning some computational tools (e.g. OBScore, ParCrys, CrystalP2, XtalPred, PPCPred, SCMCRY, SVMCRY, PredPPCrys I & II, CrysAlis I & II) that focus on feature extraction of protein sequences to predict crystallization propensity.<sup>2,116,117</sup> Considerable developments are rapidly emerging alongside the recent advances in Artificial Intelligence (AI),<sup>118–121</sup> which includes deep-learning models such as DeepSolUE,<sup>115</sup> ProteinBERT,<sup>122</sup> DSResSol,<sup>123</sup> PON-Sol2,<sup>124</sup> and DeepSol.<sup>125</sup>

## Author contributions

Joana Ferreira: conceptualization, methodology, investigation, writing – original draft. Filipa Castro: conceptualization, methodology, investigation, writing – original draft.

## Conflicts of interest

There are no conflicts to declare.

## Acknowledgements

J. Ferreira acknowledges funding from CEFT under FCT/MCTES (PIDDAC) through a postdoctoral scholarship. F. Castro acknowledges FCT CEEC Individual contract (2022.06818. CEECIND). This work was financially supported by: HealthyWaters (NORTE-01-0145-FEDER-000069), supported by Norte Portugal Regional Operational Programme (NORTE 2020), under the PORTUGAL 2020 Partnership Agreement, through the European Regional Development Fund (ERDF); and LA/P/0045/2020 (ALiCE), UIDB/00532/2020 and UIDP/00532/2020 (CEFT), funded by national funds through FCT/MCTES (PIDDAC).

## References

- H. M. Berman, J. Westbrook, Z. Feng, G. Gilliland, T. N. Bhat, H. Weissig, I. N. Shindyalov and P. E. Bourne, *Nucleic Acids Res.*, 2000, **28**, 235–242.
- C. Jin, Z. Shi, C. Kang, K. Lin and H. Zhang, *Int. J. Mol. Sci.*, 2022, **23**, 1–12.
- PDB data distribution by experimental method and molecular type, <https://www.rcsb.org/stats/summary>, (accessed 14 July 2023).
- S. C. Shoemaker and N. Ando, *Biochemistry*, 2018, **57**, 277–285.
- L. Maveyraud and L. Mourey, *Molecules*, 2020, **25**, 1–18.
- R. dos Santos, A. L. Carvalho and A. C. A. Roque, *Biotechnol. Adv.*, 2017, **35**, 41–50.
- S. Puhl, L. Meinel and O. Germershaus, *Asian J. Pharm. Sci.*, 2016, **11**, 469–477.
- D. Hekmat, D. Hebel and D. Weuster-Botz, *Chem. Eng. Technol.*, 2008, **31**, 911–916.
- E. K. Lee and W. Kim, in *Isolation and Purification of Proteins*, ed. R. Hatti-Kaul and B. Mattiasson, CRC Press, New York, Basel, 2003, pp. 1–43.
- C. N. Nanev, *Prog. Cryst. Growth Charact. Mater.*, 2020, **66**, 1–23.
- J. Newman, E. E. Bolton, J. Müller-Dieckmann, V. J. Fazio, D. T. Gallagher, D. Lovell, J. R. Luft, T. S. Peat, D. Ratcliffe, R. A. Sayle, E. H. Snell, K. Taylor, P. Vallotton, S. Velanker and F. Von Delft, *Acta Crystallogr., Sect. F: Struct. Biol. Cryst. Commun.*, 2012, **68**, 253–258.
- B. Rupp, *Acta Crystallogr., Sect. F: Struct. Biol. Commun.*, 2015, **71**, 247–260.
- J. Leng and J.-B. Salmon, *Lab Chip*, 2009, **9**, 24–34.
- S. Black, L. Dang, C. Liu and H. Wei, *Org. Process Res. Dev.*, 2013, **17**, 486–492.
- E. Saridakis and N. E. Chayen, *Biophys. J.*, 2003, **84**, 1218–1222.
- Dimensions AI, <https://app.dimensions.ai/discover/publication>, (accessed 14 July 2023).
- A. McPherson and J. A. Gavira, *Acta Crystallogr., Sect. F: Struct. Biol. Commun.*, 2014, **70**, 2–20.
- Z. S. Derewenda, *Acta Crystallogr., Sect. D: Biol. Crystallogr.*, 2010, **66**, 604–615.
- W. K. Ranatunga, D. Su and M. F. Romero, in *Molecular Life Sciences*, ed. R. D. Wells, J. S. Bond, J. Klinman and B. S. S. Masters, Springer, New York, NY, 2018, pp. 841–848.
- J. J. Mcmanus, P. Charbonneau, E. Zaccarelli and N. Asherie, *Curr. Opin. Colloid Interface Sci.*, 2016, **22**, 73–79.
- A. Ducruix and R. Giegé, *Crystallization of Nucleic Acids and Proteins – A Practical Approach*, Oxford University Press, 1999, pp. 1–435.
- L. J. Quang, S. I. Sandler and A. M. Lenhoff, *J. Chem. Theory Comput.*, 2014, **10**, 835–845.
- D. Fusco, J. J. Headd, A. De Simone, J. Wang and P. Charbonneau, *Soft Matter*, 2014, **10**, 290–302.
- K. Kubiak-Ossowska, M. Cwieka, A. Kaczynska, B. Jachimaska and P. A. Mulheran, *Phys. Chem. Chem. Phys.*, 2015, **17**, 24070–24077.
- M. Ptak-Kaczor, M. Banach, K. Stapor, P. Fabian, L. Konieczny and I. Roterman, *Int. J. Mol. Sci.*, 2021, **22**, 1–18.
- J. A. Carver, A. B. Grosas, H. Ecroyd and R. A. Quinlan, *Cell Stress Chaperones*, 2017, **22**, 627–638.



- 27 F. L. V. Gray, M. J. Murai, J. Grembecka and T. Cierpicki, *Protein Sci.*, 2012, **21**, 1954–1960.
- 28 Z. S. Derewenda and A. Godzik, *The “sticky patch” model of crystallization and modification of proteins for enhanced crystallizability*, 2017, vol. 1607, pp. 77–115.
- 29 M. Cieřlik and Z. S. Derewenda, *Acta Crystallogr., Sect. D: Biol. Crystallogr.*, 2009, **65**, 500–509.
- 30 W. N. Price, Y. Chen, S. K. Handelman, H. Neely, R. Karlin, R. Nair, J. Liu, M. Baran, S. N. Tong, F. Forouhar, S. S. Swaminathan, R. Xiao, J. R. Luft, A. Lauricella, G. T. Detitta, B. Rost, G. T. Montelione and J. F. Hunt, *Nat. Biotechnol.*, 2010, **27**, 51–57.
- 31 M. Buck, J. Boyd, C. Redfield, C. M. Dobson, D. A. MacKenzie, D. J. Jeenes and D. B. Archer, *Biochemistry*, 1995, **34**, 4041–4055.
- 32 B. Raynal, P. Lenormand, B. Baron, S. Hoos and P. England, *Microb. Cell Fact.*, 2010, **13**, 1–10.
- 33 U. Nobbmann, M. Connah, B. Fish, P. Varley, C. Gee, S. Mulot, J. Chen, L. Zhou, Y. Lu, F. Sheng, J. Yi and S. E. Harding, *Biotechnol. Genet. Eng. Rev.*, 2007, **24**, 117–128.
- 34 Y. Wang, N. van Oosterwijk, A. M. Ali, A. Adawy, A. L. Anindya, A. S. S. Dömling and M. R. Groves, *Sci. Rep.*, 2017, **7**, 1–10.
- 35 M. Dreydoppel, J. Balbach and U. Weininger, *J. Biomol. NMR*, 2022, **76**, 3–15.
- 36 J. W. Mullin, *Crystallization*, Oxford, United Kingdom, 4th edn, 2001, pp. 1–594.
- 37 C. N. Pace, F. Vajdos, L. Fee, G. Grimsley and T. Gray, *Protein Sci.*, 1995, **4**, 2411–2423.
- 38 J. E. Noble, in *Methods in Enzymology*, Edited by Press, Academic, 2014, vol. 536, pp. 17–26.
- 39 K. Zheng, L. Wu, Z. He, B. Yang and Y. Yang, *Measurement*, 2017, **112**, 16–21.
- 40 J. R. Wiřniewski and F. Z. Gaugaz, *Anal. Chem.*, 2015, **87**, 4110–4116.
- 41 Y. Etzion, R. Linker, U. Cogan and I. Shmulevich, *J. Dairy Sci.*, 2004, **87**, 2779–2788.
- 42 T. Detoisien, M. Forite, P. Taulelle, J. Teston, D. Colson, J. P. Klein and S. Veesler, *Org. Process Res. Dev.*, 2009, **13**, 1338–1342.
- 43 L. Bergeron, L. F. Filobelo, O. Galkin and P. G. Vekilov, *Biophys. J.*, 2003, **85**, 3935–3942.
- 44 J. P. Guilloteau, M. M. Riès-Kautt and A. F. Ducruix, *J. Cryst. Growth*, 1992, **122**, 223–230.
- 45 S. B. Howard, P. J. Twigg, J. K. Baird and E. J. Meehan, *J. Cryst. Growth*, 1988, **90**, 94–104.
- 46 E. L. Forsythe, R. A. Judge and M. L. Pusey, *J. Chem. Eng. Data*, 1999, **44**, 637–640.
- 47 A. P. Golovanov, G. M. Hautbergue, S. A. Wilson and L. Y. Lian, *J. Am. Chem. Soc.*, 2004, **126**, 8933–8939.
- 48 S. R. Trevino, J. M. Scholtz and C. N. Pace, *J. Pharm. Sci.*, 2008, **97**, 4155–4166.
- 49 N. E. Chayen, P. D. Shaw Stewart, D. L. Maeder and D. M. Blow, *J. Appl. Crystallogr.*, 1990, **23**, 297–302.
- 50 S. Talreja, S. L. Perry, S. Guha, V. Bhamidi, C. F. Zukoski and P. J. A. Kenis, *J. Phys. Chem. B*, 2010, **114**, 4432–4441.
- 51 N. Asherie, *Methods*, 2004, **34**, 266–272.
- 52 M. L. Pusey and K. Gernert, *J. Cryst. Growth*, 1988, **88**, 419–424.
- 53 E. Cacioppo, S. Munson and M. L. Pusey, *J. Cryst. Growth*, 1991, **110**, 66–71.
- 54 K. Nakazato, T. Homma and T. Tomo, *J. Synchrotron Radiat.*, 2004, **11**, 34–37.
- 55 L. F. Haire and D. M. Blow, *J. Cryst. Growth*, 2001, **232**, 17–20.
- 56 W. Iwai, D. Yagi, T. Ishikawa, Y. Ohnishi, I. Tanaka and N. Niimura, *J. Synchrotron Radiat.*, 2008, **15**, 312–315.
- 57 D. L. Chen, G. J. Gerdtz and R. F. Ismagilov, *J. Am. Chem. Soc.*, 2005, **127**, 9672–9673.
- 58 I. Broutin, M. Riès-Kautt and A. Ducruix, *J. Appl. Crystallogr.*, 1995, **28**, 614–617.
- 59 A. Adawy, K. Marks, W. J. de Grip, W. J. P. van Enckevort and E. Vlieg, *CrystEngComm*, 2013, **15**, 2275–2286.
- 60 C. Ferreira, M. F. Pinto, S. Macedo-Ribeiro, P. J. B. Pereira, F. A. Rocha and P. M. Martins, *Phys. Chem. Chem. Phys.*, 2020, **22**, 16143–16149.
- 61 A. R. Feeling-Taylor, R. Michael Banish, R. E. Hirsch and P. G. Vekilov, *Rev. Sci. Instrum.*, 1999, **70**, 2845–2849.
- 62 R. J. Gray, W. B. Hou, A. B. Kudryavtsev and L. J. DeLucas, *J. Cryst. Growth*, 2001, **232**, 10–16.
- 63 A. E. S. van Driessche, J. A. Gavira, L. D. Patiño Lopez and F. Otalora, *J. Cryst. Growth*, 2009, **311**, 3479–3484.
- 64 S. Santesson, E. S. Cedergren-Zeppezauer, T. Johansson, T. Laurell, J. Nilsson and S. Nilsson, *Anal. Chem.*, 2003, **75**, 1733–1740.
- 65 M. Hofmann, M. Winzer, C. Weber and H. Gieseler, *J. Pharm. Pharmacol.*, 2018, **70**, 648–654.
- 66 M. Oeller, P. Sormanni and M. Vendruscolo, *Sci. Rep.*, 2021, **11**, 1–10.
- 67 Q. Chai, J. Shih, C. Weldon, S. Phan and B. E. Jones, *mAbs*, 2019, **11**, 747–756.
- 68 R. M. Kramer, V. R. Shende, N. Motl, C. N. Pace and J. M. Scholtz, *Biophys. J.*, 2012, **102**, 1907–1915.
- 69 I. R. M. Juckes, *Biochim. Biophys. Acta*, 1971, **229**, 535–546.
- 70 M. C. R. Heijna, W. J. P. van Enckevort and E. Vlieg, *Phys. Rev. E: Stat., Nonlinear, Soft Matter Phys.*, 2007, **76**, 1–7.
- 71 Y.-C. Shih, J. M. Prausnitz and H. W. Blanch, *Biotechnol. Bioeng.*, 1992, **40**, 1155–1164.
- 72 B. C. Hancock and M. Parks, *Pharm. Res.*, 2000, **17**, 397–404.
- 73 G. Peybernès, R. Grossier, F. Villard, P. Letellier, M. Lagaize, N. Candoni and S. Veesler, *Org. Process Res. Dev.*, 2018, **22**, 1856–1860.
- 74 G. Peybernès, R. Grossier, F. Villard, P. Letellier, N. Candoni and S. Veesler, *Cryst. Growth Des.*, 2020, **20**, 3882–3887.
- 75 F. J. Link and J. Y. Y. Heng, *CrystEngComm*, 2021, **23**, 3951–3960.
- 76 F. J. Link and J. Y. Y. Heng, *Cryst. Growth Des.*, 2022, **22**, 3024–3033.
- 77 G. Sazaki, K. Kurihara, T. Nakada, S. Miyashita and H. Komatsu, *J. Cryst. Growth*, 1996, **169**, 355–360.
- 78 M. Wiendahl, C. Völker, I. Husemann, J. Krarup, A. Staby, S. Scholl and J. Hubbuch, *Chem. Eng. Sci.*, 2009, **64**, 3778–3788.





- 79 D. Wei, M. Wang, H. Wang, G. Liu, J. Fang and Y. Jiang, *ACS Omega*, 2022, **7**, 31338–31347.
- 80 W. W. Wilson and L. J. Delucas, *Acta Crystallogr., Sect. F: Struct. Biol. Commun.*, 2014, **70**, 543–554.
- 81 L. Hentschel, J. Hansen, S. U. Egelhaaf and F. Platten, *Phys. Chem. Chem. Phys.*, 2021, **23**, 2686–2696.
- 82 B. L. Neal, D. Asthagiri, O. D. Velev, A. M. Lenhoff and E. W. Kaler, *J. Cryst. Growth*, 1999, **196**, 377–387.
- 83 M. Dieterle, T. Blaschke and H. Hasse, *Z. Phys. Chem.*, 2013, **227**, 333–343.
- 84 S. Ruppert, S. I. Sandler and A. M. Lenhoff, *Biotechnol. Prog.*, 2001, **17**, 182–187.
- 85 C. M. Mehta, E. T. White and J. D. Litster, *Biotechnol. Prog.*, 2012, **28**, 163–170.
- 86 B. Guo, S. Kao, H. McDonald, A. Asanov, L. L. Combs and W. W. Wilson, *J. Cryst. Growth*, 1999, **196**, 424–433.
- 87 W. W. Wilson, *J. Struct. Biol.*, 2003, **142**, 56–65.
- 88 A. Quigley and D. R. Williams, *Eur. J. Pharm. Biopharm.*, 2015, **96**, 282–290.
- 89 A. Adawy and M. R. Groves, *Crystals*, 2017, **7**, 1–10.
- 90 E. Binabaji, S. Rao and A. L. Zydney, *Biotechnol. Bioeng.*, 2014, **111**, 529–536.
- 91 S. K. Chaturvedi and P. Schuck, *AAPS J.*, 2019, **21**, 1–9.
- 92 A. Saluja, R. M. Fesinmeyer, S. Hogan, D. N. Brems and Y. R. Gokarn, *Biophys. J.*, 2010, **99**, 2657–2665.
- 93 K. K. Arthur, J. P. Cabirelson, B. S. Kendrick and M. R. Stoner, *J. Pharm. Sci.*, 2009, **98**, 3522–3539.
- 94 Y. Liu, X. Wang and C. B. Ching, *Cryst. Growth Des.*, 2010, **10**, 548–558.
- 95 E. Pantuso, T. F. Mastropietro, M. L. Briuglia, C. J. J. Gerard, E. Curcio, J. H. ter Horst, F. P. Nicoletta and G. Di Profio, *Sci. Rep.*, 2020, **10**, 1–14.
- 96 P. M. Tessier and A. M. Lenhoff, *Curr. Opin. Biotechnol.*, 2003, **14**, 512–516.
- 97 J. J. Valente, K. S. Verma, M. C. Manning, W. W. Wilson and C. S. Henry, *Biophys. J.*, 2005, **89**, 4211–4218.
- 98 Z. S. Derewenda and P. G. Vekilov, *Acta Crystallogr., Sect. D: Biol. Crystallogr.*, 2006, **62**, 116–124.
- 99 C.-B. Lu, J. Wang and X.-J. Ching, *Cryst. Growth Des.*, 2003, **3**, 83–87.
- 100 J. Ferreira, F. Castro, F. Rocha and S. Kuhn, *Chem. Eng. Sci.*, 2018, **191**, 232–244.
- 101 E. A. Stura, G. R. Nemerow and I. A. Wilson, *J. Cryst. Growth*, 1992, **122**, 273–285.
- 102 G. M. Whitesides, *Nature*, 2006, **442**, 368–373.
- 103 S. Haerberle and R. Zengerle, *Lab Chip*, 2007, **7**, 1094–1110.
- 104 M. O. A. Sommer and S. Larsen, *J. Synchrotron Radiat.*, 2005, **12**, 779–785.
- 105 N. Candoni, R. Grossier, M. Lagaize and S. Veessler, *Annu. Rev. Chem. Biomol. Eng.*, 2019, **10**, 59–83.
- 106 S. Maosoongnern, V. Diaz Borbon, A. E. Flood and J. Ulrich, *Ind. Eng. Chem. Res.*, 2012, **51**, 15251–15257.
- 107 M. Ildefonso, N. Candoni and S. Veessler, *Cryst. Growth Des.*, 2011, **11**, 1527–1530.
- 108 N. Junius, S. Jaho, Y. Sallaz-Damaz, F. Borel, J. B. Salmon and M. Budayova-Spano, *Lab Chip*, 2020, **20**, 296–310.
- 109 C. L. Hansen, M. O. A. Sommer and S. R. Quake, *Proc. Natl. Acad. Sci. U. S. A.*, 2004, **101**, 14431–14436.
- 110 M. A. Reus, A. E. D. M. Van Der Heijden and J. H. Ter Horst, *Org. Process Res. Dev.*, 2015, **19**, 1004–1011.
- 111 Technobis Group, Technobis Crystallization Systems, <https://www.crystallizationsystems.com/applications/solubility/>, (accessed 22 June 2023).
- 112 J. H. ter Horst, M. A. Deij and P. W. Cains, *Cryst. Growth Des.*, 2009, **9**, 1531–1537.
- 113 M. Oeller, R. Kang, R. Bell, H. Ausserwöger, P. Sormanni and M. Vendruscolo, *Briefings Bioinf.*, 2023, **24**, 1–7.
- 114 M. Hebditch, M. A. Carballo-Amador, S. Charonis, R. Curtis and J. Warwicker, *Bioinformatics*, 2017, **33**, 3098–3100.
- 115 C. Wang and Q. Zou, *BMC Biol.*, 2023, **21**, 1–11.
- 116 A. Elbasir, R. Mall, K. Kunji, R. Rawi, Z. Islam, G. Y. Chuang, P. R. Kolatkar and H. Bensmail, *Bioinformatics*, 2020, **36**, 1429–1438.
- 117 H. Wang, L. Feng, G. I. Webb, L. Kurgan, J. Song and D. Lin, *Briefings Bioinf.*, 2018, **19**, 838–852.
- 118 K. Suzuki, K. Sakakibara, M. Nakamura, S. Shinoda and Y. Asano, in *Proceedings of the International Conference on Machine Learning and Cybernetics*, IEEE Computer Society, 2022, vol. 2022-September, pp. 237–241.
- 119 J. Chen, S. Zheng, H. Zhao and Y. Yang, *J. Cheminf.*, 2021, **13**, 1–10.
- 120 X. Han, W. Ning, X. Ma, X. Wang and K. Zhou, *Metab. Eng. Commun.*, 2020, **11**, 1–9.
- 121 X. Han, X. Wang and K. Zhou, *Bioinformatics*, 2019, **35**, 4640–4646.
- 122 N. Brandes, D. Ofer, Y. Peleg, N. Rappoport and M. Linial, *Bioinformatics*, 2022, **38**, 2102–2110.
- 123 M. Madani, K. Lin and A. Tarakanova, *Int. J. Mol. Sci.*, 2021, **22**, 1–20.
- 124 Y. Yang, L. Zeng and M. Vihinen, *Int. J. Mol. Sci.*, 2021, **22**, 1–15.
- 125 S. Khurana, R. Rawi, K. Kunji, G.-Y. Chuang, H. Bensmail and R. Mall, *Bioinformatics*, 2018, **34**, 2605–2613.

